State-selective electron capture in collisions of ground and metastable N²⁺ ions with H(1*s*)

P. Barragán, L. F. Errea, L. Méndez, A. Macías,* I. Rabadán,† and A. Riera

Laboratorio Asociado al CIEMAT de Física Atómica y Molecular en Plasmas de Fusión, Departamento de Química,
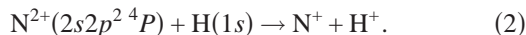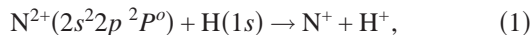*Universidad Autónoma de Madrid, Madrid-28049, Spain*

An *ab initio* calculation of the electron capture cross sections for collisions of ground and metastable states of N²⁺ with H(1*s*) is presented. Total cross sections are evaluated for ¹⁴N impact energies from 2×10^{-3} to 300 keV, using both quantal and semiclassical treatments. The results are compared with experimental and previous theoretical data, and are used to check the presence of metastable ions in the beams employed in the experiments. Partial cross sections are also presented and related to the collision mechanism.

DOI: 10.1103/PhysRevA.70.022707   PACS number(s): 34.70.+e, 34.10.+x

I. INTRODUCTION

Electron capture (EC) in ion-atom (-molecule) collisions is important in astrophysical and fusion plasmas. However, the measurement of cross sections for these processes is often difficult due to the presence of unknown quantities of metastable species in the ion beam, and only recently have double translational energy techniques allowed measurement of EC cross sections for ions in both ground and metastable states (see [1,2]). In particular, N²⁺ beams from the usual ion sources are, in principle, a mixture of unknown proportions of ground state $(2s^2 2p\ ^2P^o)$ and metastable $(2s2p^2\ ^4P)$ ions and, accordingly, the following EC reactions can take place in N²⁺+H collisional experiments:

$$N^{2+}(2s^2 2p\ ^2P^o) + H(1s) \rightarrow N^+ + H^+, \qquad (1)$$

$$N^{2+}(2s2p^2\ ^4P) + H(1s) \rightarrow N^+ + H^+. \qquad (2)$$

Experimental work on this system includes the measurements of total EC cross sections of Refs. [3,4], carried out with a mixed beam, for ¹⁴N impact energies (E) in the range 8–600 keV. Translational energy experiments [5], which also used a mixed beam, yielded state-selective EC cross sections in the energy range 0.6–8 keV, extending the range to 200 keV for total EC cross sections. The use of the double translational energy spectroscopy technique allowed the energy change spectrum in EC to be recorded for an incident pure beam of ground state ions, at five collision energies between 0.8 and 6 keV [2]; these spectra showed three peaks at $\Delta E \simeq 4.6$, 2.5, and -2 eV, corresponding to EC into $N^+(2s2p^3\ ^3D^o)$, $N^+(2s2p^3\ ^3P^o)$, and $N^+(2s^2 2p3s\ ^1P^o$ or $^3P^o)$, respectively.

Pieksma *et al.* [6] carried out merged-beam measurements in a wide energy range 1.4×10^{-3}–62.2 keV. The measured total cross sections agree with previous experiments at $E > 30$ eV, but there are important disagreements at lower energies; e.g., differences of the order of 25% are found at

$E \simeq 10$ keV, and there is a shift to lower energies ($E \simeq 2$ keV) of the local maximum found by Wilkie *et al.* [5] at $E \simeq 5$ keV. This discrepancy is tentatively ascribed in [6] to the presence of vibrationally excited H_2 in the experiment of Ref. [5].

Theoretical works on N²⁺+H collisions include the two-state calculation of Refs. [7,8], in the range of impact energies from 8.1×10^{-5} to 80.4 keV. Herrero *et al.* [9] performed a quantal close-coupling calculation (triplets only) for $E < 1$ keV, which yielded total cross sections in reasonable agreement with the experimental data of Ref. [6], except for a maximum of the calculated cross section at $E \simeq 4$ eV, not found in the experiment. Also, the energy dependence of cross section of Ref. [9] is completely different from the experimental one of Ref. [5] in the region $0.6 < E < 1$ keV.

The aim of the present paper is to present an extended close-coupling calculation of state-selective EC cross section for energies up to 300 keV. The calculation in the range $1 < E < 300$ keV, not covered by the work of Herrero *et al.* [9], requires the use of a large molecular basis set in order to consider collisions from both ground and metastable ions. In this energy range, we have employed the techniques previously applied to C²⁺+H [10] and O²⁺+H [11] collisions, which used a semiclassical treatment in terms of molecular expansions. For $E \simeq 1$ keV, since there exists a discrepancy between measured and calculated total cross sections, and also between values from different experiments, we have employed both semiclassical and quantal treatments. This calculation is also relevant from the theoretical point of view since semiclassical and quantal results have been compared only for a few collisions. The energy region $0.002 < E < 1$ keV was covered by the calculation of [9] for reaction (1), but, given the sensitivity of the cross sections to the quality of the molecular data, we have extended the energy range down to 2 eV to check those results, in particular the different slope of the total cross sections when compared with the merged-beam results [6] and the above-mentioned maximum of the EC total cross section at $E \simeq 4$ eV. In addition, the calculation of partial cross sections is particularly relevant at low energy, where present experimental techniques (merged-beam experiments [12]) yield only total cross sections, and new calculations have been recently carried out for one-electron systems (see Ref. [13] and references therein).

---

*Also at Instituto de Estructura de la Materia, CSIC, Serrano 123, Madrid-28006, Spain.

†Author to whom correspondence should be addressed. Electronic address: Ismanuel.Rabadan@uam.es

The paper is organized as follows. In Sec. II we summarize the dynamical (quantal and semiclassical) methods employed in the calculation. The details of the molecular calculation are presented in Sec. III and the dynamical calculations in Sec. IV. Our main conclusions are outlined in Sec. V. Cross sections are plotted as functions of ^{14}N impact energy in keV. Atomic units are used unless otherwise indicated.

II. METHOD

A. Quantal treatment

For energies below 1 keV, we have applied a quantal treatment with a common reaction coordinate (CRC) [14,15]. In this section we only summarize the basis of the CRC method. A more detailed account of our implementation and references to previous works can be found in Ref. [16]. In the CRC treatment, the scattering wave function Ψ^J is expanded in a molecular basis set $\{\phi_j\}$. For each value of the total angular momentum J, one writes

$$\Psi^J(\mathbf{r},\boldsymbol{\xi}) = \sum_k \chi_k^J(\boldsymbol{\xi})\phi_k(\mathbf{r},\boldsymbol{\xi}), \tag{3}$$

where $\mathbf{r}$ denotes the set of electronic coordinates and the functions ϕ_k are approximate eigenfunctions of the clamped-nuclei electronic Hamiltonian:

$$H_{\text{elec}}\phi_k(\mathbf{r},\xi) = \epsilon_k(\xi)\phi_k(\mathbf{r},\xi). \tag{4}$$

In Eqs. (3) and (4), $\boldsymbol{\xi}$ is the CRC, which ensures that a truncated expansion satisfies the scattering boundary conditions; this coordinate is a combination of electronic and nuclear coordinates of the form

$$\boldsymbol{\xi} = \mathbf{R} + \frac{1}{\mu}\mathbf{s}(\mathbf{r},R) \tag{5}$$

with

$$\mathbf{s} = \sum_{\alpha=1}^{N_{\text{elec}}} \left[f(\mathbf{r}_\alpha,R)\mathbf{r}_\alpha - \frac{1}{2}f^2(\mathbf{r}_\alpha,R)\mathbf{R} \right]. \tag{6}$$

In these expressions, μ is the nuclear reduced mass, $\mathbf{R}$ is the internuclear vector, N_{elec} is the number of electrons, $\mathbf{r}_\alpha$ are the electronic position vectors, relative to the center of mass of the nuclei, and f is a switching function which satisfies

$$\lim_{R\to\infty, r_{\alpha A},\text{ finite}} f(\mathbf{r}_\alpha,R) = -p,$$

$$\lim_{R\to\infty, r_{\alpha B},\text{ finite}} f(\mathbf{r}_\alpha,R) = q, \tag{7}$$

where pR and qR are, respectively, the distances from nuclei A and B to the center of nuclear mass. It can be shown that, for any reaction channel, the CRC of expression (5) becomes the appropriate asymptotic interatomic coordinate to $\mathcal{O}(\mu^{-1})$. Substitution of the expansion (3) in the stationary Schrödinger equation yields a system of differential equations for the nuclear wave functions

$$[(2\mu^{-1})\nabla_\xi^2 + (\mathcal{E} - \epsilon_j)]\chi_j^J + \sum_l [2\mu^{-1}\mathbf{M}_{jl}\cdot\boldsymbol{\nabla}_\xi + \langle\phi_j|\nabla_\xi^2|\phi_l\rangle]\chi_l^J$$

$$= 0, \tag{8}$$

where $\mathcal{E}$ is the impact energy in the center of mass reference frame. Terms proportional to v^2 have been neglected in Eq. (8), and the modified dynamical coupling $\mathbf{M}_{jl}$ is a vector whose q component has the form

$$M_{jl}^q = \langle\phi_j|\frac{\partial}{\partial\xi_q}|\phi_l\rangle + A_{jl}^q \tag{9}$$

with

$$A_{jl}^q = \sum_{\alpha=1}^{N_{\text{elec}}} \langle\phi_j|\boldsymbol{\nabla}_{\mathbf{r}_\alpha}(s_q)\cdot\boldsymbol{\nabla}_{\mathbf{r}_\alpha} + \nabla_{\mathbf{r}_\alpha}^2(s_q)|\phi_l\rangle. \tag{10}$$

The form of the corrections $\mathbf{A}_{jl}$ depends on the particular switching function employed. In this work we have used that of [17]:

$$f(\mathbf{r}_j,R) = \frac{R}{R^2+\beta^2}\mathbf{r}_j\cdot\hat{\mathbf{R}}, \tag{11}$$

which has been employed in several works for many-electron collision systems. The nuclear wave functions χ_j are obtained by solving numerically the system of differential equations (8). From these solutions, the elements of the **S**-matrix are then calulated using standard collision theory, and the total cross section for the $i \to j$ transition, σ_{ij}, is given by

$$\sigma_{ij} = \frac{\pi}{k_i^2}\sum_J (2J+1)|S_{ij}^J|^2, \tag{12}$$

where k_i is the initial linear momentum.

B. Semiclassical treatments

For impact energies above 1 keV, we employ the impact-parameter method (see e.g. [18]), where the nuclei follow straight-line trajectories with constant relative velocity $\mathbf{v}$ and impact parameter $\mathbf{b}$ ($\mathbf{R} = \mathbf{b} + \mathbf{v}t$), while the electronic motion is described by the wavefunction $\boldsymbol{\Psi}^{\text{SC}}(\mathbf{r},t;b,v)$, which is a solution of the equation

$$\left(H_{\text{elec}} - i\frac{\partial}{\partial t}\bigg|_\mathbf{r} \right)\Psi^{\text{SC}}(\mathbf{r},t;b,v) = 0 \tag{13}$$

and is expanded as

$$\Psi^{\text{SC}} = D(\mathbf{r},R)\sum_j a_j(t;b,v)\phi_j(\mathbf{r},R)\exp\left[-i\int_0^t \epsilon_j dt' \right], \tag{14}$$

where D is a common translation factor (CTF) [19]:

$$D(\mathbf{r},R) = \exp\left[i\sum_{\alpha}^{Nelec}\left(f(\mathbf{r}_{\alpha},\mathbf{R})\mathbf{v}\cdot\mathbf{r}_{\alpha} - \frac{1}{2}f^2(\mathbf{r}_{\alpha},R)v^2 t\right)\right].$$

$$(15)$$

It has been shown [16,20] that the CTF method, with the same switching function, can be obtained from the CRC one by applying the eikonal approximation and assuming a constant and state independent local velocity. The coefficients of the expansion are solutions of the system of differential equations

$$i\dot{a}_j = \sum_l \left[\mathbf{v}\cdot\mathbf{M}_{jl} + v^2 B_{jl}\right]a_l \exp\left[-i\int_0^t (\epsilon_l - \epsilon_j)dt'\right],$$

$$(16)$$

where $\mathbf{M}_{jl}$ has been defined in Eqs. (9) and (10) and B_{jl} are terms whose explicit form can be found in [19]. The radial and rotational components of the modified dynamical couplings are

$$R_{jl} = \left\langle \phi_j \left| \frac{\partial}{\partial R} \right| \phi_l \right\rangle + A_{jl}^R \qquad (17)$$

and

$$L_{jl} = \left\langle \phi_j \left| \sum_{\alpha}^{Nelec} iL_y(\mathbf{r}_{\alpha}) \right| \phi_l \right\rangle + A_{jl}^{\theta}, \qquad (18)$$

where L_y is the Y component of the electronic angular momentum operator.

The total cross section is given by

$$\sigma_{ij}(v) = 2\pi \int_0^{\infty} bP_{ij}(b,v)db \qquad (19)$$

where the probability P_{ij} for transition to the final state ψ_j is calculated from the coefficient a_j of expansion (14):

$$P_{ij}(b,v) = \lim_{t\to\infty}|\langle\psi_j|\Psi\rangle - \delta_{ij}|^2 = \lim_{t\to\infty}|a_j(t;b,v) - \delta_{ij}|^2.$$

$$(20)$$

The quantal and semiclassical transition probabilities are related by [see Eqs. (12) and (19)]

$$bP_{ij}(b) = \frac{(2J+1)}{2k_i}|S_{ij}^J|^2 \qquad (21)$$

with $b=J/k_i$

III. MOLECULAR CALCULATIONS

The entrance channel of reaction (1) is a statistical mixture of singlet and triplet molecular states, while that of reaction (2) contains triplet and quintet states. Accordingly, we have calculated the electronic energies for states of the quasimolecule NH^{2+} with these multiplicities.

Molecular states ϕ_j and energies ϵ_j have been calculated using a multireference configuration interaction method (MRCI) with the program MELD [21]. This method starts with a SCF calculation in a basis of Gaussian type orbitals

TABLE I. Comparison of N^+ and N^{2+} energy differences ($E_i - E_1$ for singlet and triplet states and $E_i - E_2$ for quintets, in eV) with experimental ones [22]. Also, the molecular states (MS) of the NH^{2+} quasimolecule to which the atomic states correlate.

i	Channel	This work	Ref. [22]	MS
1	$N^{2+}(2s^2 2p\ ^2P^o)$	0.000	0.000	$^{1,3}\Sigma^+,\ ^{1,3}\Pi$
2	$N^{2+}(2s2p^2\ ^4P)$	7.045	7.090	$^{3,5}\Sigma^-,\ ^{3,5}\Pi$
3	$N^{2+}(2s2p^2\ ^2D)$	12.410	12.525	$^{1,3}\Sigma^+,\ ^{1,3}\Pi,\ ^{1,3}\Delta$
4	$N^{2+}(2s2p^2\ ^2S)$	16.219	16.242	$^{1,3}\Sigma^+$
5	$N^+(2s^2 2p^2\ ^3P)$	−29.470	−29.600	$^3\Sigma^-,\ ^3\Pi$
6	$N^+(2s^2 2p^2\ ^1D)$	−27.512	−27.701	$^1\Sigma^+,\ ^1\Pi,\ ^1\Delta$
7	$N^+(2s^2 2p^2\ ^1S)$	−25.337	−25.547	$^1\Sigma^+$
8	$N^+(2s2p^3\ ^3D^o)$	−17.976	−18.164	$^3\Sigma^-,\ ^3\Pi,\ ^3\Delta$
9	$N^+(2s2p^3\ ^3P^o)$	−15.856	−16.059	$^3\Sigma^+,\ ^3\Pi$
10	$N^+(2s2p^3\ ^1D^o)$	−11.369	−11.723	$^1\Sigma^-,\ ^1\Pi,\ ^1\Delta$
11	$N^+(2s^2 2p3s\ ^3P^o)$	−11.102	−11.138	$^3\Sigma^+,\ ^3\Pi$
12	$N^+(2s^2 2p3s\ ^1P^o)$	−11.050	−11.103	$^1\Sigma^+,\ ^1\Pi$
13	$N^+(2s2p^3\ ^3S^o)$	−9.996	−10.367	$^3\Sigma^-$
14	$N^+(2s^2 2p3p\ ^1P)$	−9.143	−9.191	$^1\Sigma^-,\ ^1\Pi$
15	$N^+(2s^2 2p3p\ ^3D)$	−8.906	−8.954	$^3\Sigma^+,\ ^3\Pi,\ ^3\Delta$
16	$N^+(2s2p^3\ ^1P^o)$	−8.534	−8.924	$^1\Sigma^+,\ ^1\Pi$
17	$N^+(2s^2 2p3p\ ^3S)$	−8.604	−8.660	$^3\Sigma^+$
18	$N^+(2s^2 2p3p\ ^3P)$	−8.400	−8.452	$^3\Sigma^-,\ ^3\Pi$
19	$N^+(2s2p^3\ ^5S^o)$	−30.746	−30.889	$^5\Sigma^-$
20	$N^+(2s2p^2 3s\ ^5P)$	−11.190	−11.200	$^5\Sigma^-,\ ^5\Pi$
21	$N^+(2s2p^2 3p\ ^5D^o)$	−8.923	−8.963	$^5\Sigma^-,\ ^5\Pi,\ ^5\Delta$
22	$N^+(2s2p^2 3p\ ^5P^o)$	−8.669	−8.720	$^5\Sigma^+,\ ^5\Pi$

(GTOs); this provides a set of molecular orbitals (MOs) which are then used to construct the reference configurations. Each reference configuration is a symmetry- and spin-adapted linear combination of a few Slater determinants built up from products of the MOs. The configuration interaction (CI) space includes single and double excitations from the reference set. The calculations have been performed within the C_s symmetry point group, which means that Σ^+, Π_+, Δ_+, … molecular states appear as A' states while Σ^-, Π_-, Δ_-, … are A'' states, where the subindexes $\pm$ indicate the symmetry of the corresponding state under reflection in the collision plane.

In the present calculation, the GTO basis sets, centered at the N and H nuclei, were taken from [23] and consist of $\{5s,4p,3d,2f\}$ and $\{4s,3p,1d\}$ contracted GTOs, respectively. The MOs were obtained in a restricted SCF calculation for the NH^{4+} system, where the SCF configuration correlates, in the limit $R\to\infty$, to the $1s^2 2s^2$ configuration of N^{3+}, so that the $2p$ orbitals obtained are not occupied and are degenerate. The equivalence of the p orbitals helps us to describe with the same accuracy the states involved in the collision, which have different occupancies of these orbitals (see Table I). For each subsystem, the CI space was built from a set of (at most) 80 reference configurations. To limit the final number of configurations in the CI, we have applied the following restrictions: (i) Frozen core approximation: we keep only configurations with the ground MO, 1σ, doubly

occupied. (ii) Doubly excited configurations are selected using second order perturbation theory: for each subsystem, only those configurations with a contribution larger than 5×10^{-6} Hartree to the energy of any of the lowest n-zeroth-order wave functions were kept. We have taken the zeroth-order wavefunctions as the eigenvectors of the Hamiltonian matrix in the basis of reference configurations, with $n=16$ for $^3A'$ and $^3A''$ subsystems, 14 for $^1A'$, 10 for $^1A''$, 7 for $^5A'$ and 9 for $^5A''$ subsystems, respectively.

The set of reference configurations was allowed to change iteratively at each R in the following way: For each of the six subsystems, an initial guess of 80 reference configurations was generated in the limit $R \to \infty$; this set contained the basic structures of the atomic channels to be included in the dynamical calculation (those listed in Table I). Using this set we carried out a MRCI calculation, and we selected the 80 configurations with the largest contributions to the lowest 16 ($^3A'$ and $^3A''$), 14 ($^1A'$), 10 ($^1A''$), 7 ($^5A'$), and 9 ($^5A''$) states obtained in this calculation, which were then used as a new reference set, and the selection procedure was repeated. After three iterations the reference set converged and the weight of the reference configurations in the calculated CI functions was larger than 96% for the states of Table I. To ensure a similar precision of the wave functions at any internuclear distance, the selection of the reference set was repeated at each value of R, with the converged reference set at a given value of the internuclear distance R_i used as the initial guess at a nearby point R_{i+1} ($R_i > R_{i+1}$). In practice, $R_i - R_{i+1} = 0.2a_0$ a except for $R < 4a_0$ and in the regions of avoided crossings, where the step size was reduced to $0.05a_0$. The CI space included up to 3.2×10^4 Slater determinants for $^3A'$, 3.1×10^4 for $^3A''$, 1.1×10^4 for $^1A'$, 1.6×10^4 for $^1A''$, 1.6×10^3 for $^5A'$, and 1.7×10^3 for $^5A''$.

As a check of the accuracy of our calculation, we compare in Table I the calculated atomic energies [singlets and triplets relative to the ground state of N^{2+} and quintets relative to the metastable $N^{2+}(^4P)$] of the N^+ and N^{2+} states included in the dynamical calculation with the experimental values [22]. The errors in these energy differences are smaller than 0.3 eV for the relevant channels and the error in the ionization potential of $H(1s)$ is smaller than 3×10^{-3} eV; this is sufficient for the dynamical calculation. We also include in this table the symmetries of the states of the NH^{2+} quasimolecule correlating to each atomic state. Molecular states and their asymptotic atomic limit will be referred in the text according to the labels of the first column of the table.

The energies of triplet, singlet, and quintet molecular states are depicted in Figs. 1–3, respectively. In the triplet subsystem, the energies of the molecular states $1 \,^3\Sigma^+$ and $1 \,^3\Pi$, which are the entrance channels of reaction (1), show avoided crossings with those molecular states of the same symmetry correlating to channel 9 at about $R=12a_0$ and with those of channel 8 at about $R=6.5a_0$. The first ones are very narrow and have been crossed diabatically. In the singlet subsystem (Fig. 2) the energies of the entrance channels $(1 \,^1\Sigma^+, 1 \,^1\Pi)$ do not show narrow avoided crossings with those of the EC channels, and the most likely mechanism for EC in this subsystem involves $1 \,^1\Pi$–$10 \,^1\Pi$ transitions in the wide avoided crossing at $R=2a_0$.
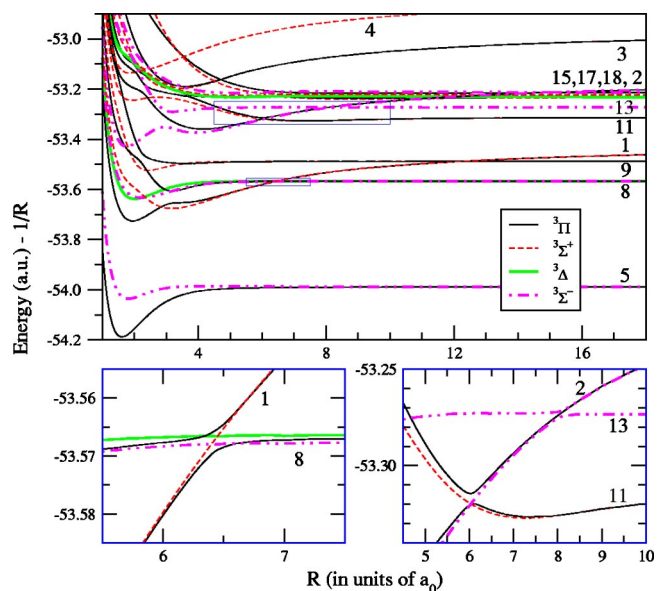

FIG. 1. Potential energy curves of $(NH)^{2+}$: triplet subsystem. Channels are labeled according to Table I. Bottom panels are expansions of the boxes marked in the top panel.

To treat reaction (2), triplet and quintet molecular states are required. In the triplet subsystem, the energies of the entrance channels of reaction (2) (states $2 \,^3\Sigma^-$ and $2 \,^3\Pi$) show very narrow avoided crossings at $R > 10a_0$ with those of molecular states dissociating into channels 15, 17, and 18, which have been crossed diabatically. At low velocities, the main mechanism of reaction (2) involves transitions in the avoided crossings with the energies of states of channels 13 and 11 at $R \simeq 8.1a_0$ and $R \simeq 6.1a_0$, respectively. On the contrary, in the quintet subsystem (Fig. 3), the energy of the entrance channel does not show any avoided crossing for $R > 2a_0$ and sizable charge exchange transitions are expected only at high energies.
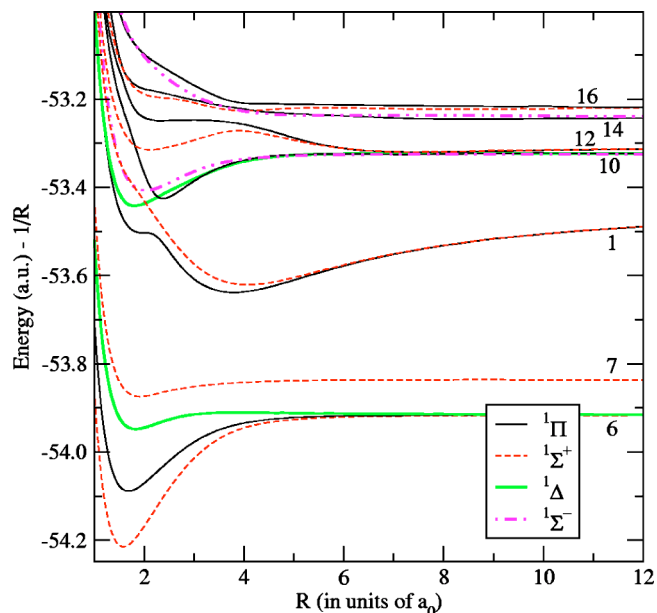

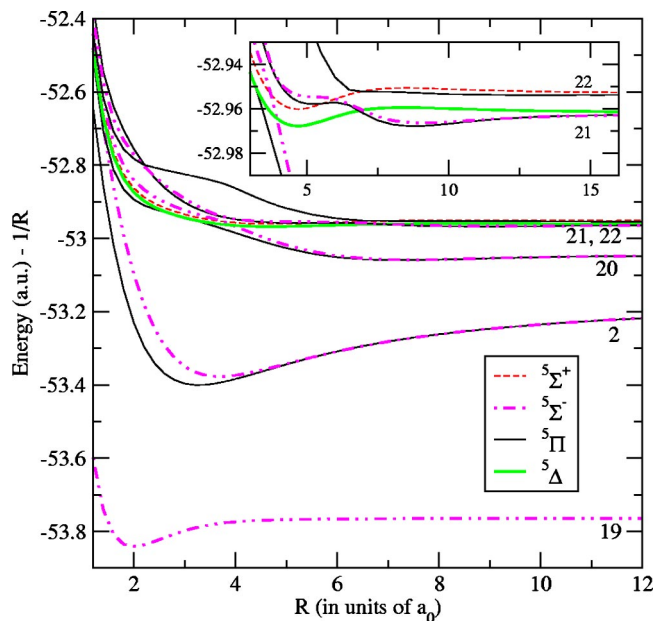FIG. 2. Potential energy curves of $(NH)^{2+}$: singlet subsystem. Channels are labeled according to Table I.

FIG. 3. Potential energy curves of $(NH)^{2+}$: quintet subsystem. Channels are labeled according to Table I.

FIG. 4. Selected redial and rotational couplings between terms of different channels in the triplet subsystem, as indicated in the panels.

The dynamical couplings of equations (17) and (18) were evaluated numerically, as explained in [24]; this method involves the calculation of the delayed overlap matrix elements $\langle \phi_i(\mathbf{R}) | \phi_j(\mathbf{R}+\boldsymbol{\delta}) \rangle$. In this work we have used $|\boldsymbol{\delta}| = 10^{-4} a_0$. An important practical difficulty in applying the molecular expansion to many-electron systems is the erratic sign of the molecular wave functions ϕ_i, which results in meaningless signs of the dynamical couplings. To solve this arbitrariness, we have implemented an algorithm to automatize the sign coherence of the molecular states ϕ_i, both between successive grid points $(\mathbf{R}_j, \mathbf{R}_{j+1})$ and in the calculation of the couplings $(\mathbf{R}_j, \mathbf{R}_j + \boldsymbol{\delta})$. This method is based on the evaluation of the delayed overlaps $\langle \phi_i(\mathbf{R}) | \phi_i(\mathbf{R}+\boldsymbol{\delta}) \rangle$ and $\langle \phi_i(\mathbf{R}_j) | \phi_i(\mathbf{R}_{j+1}) \rangle$ and will be published elsewhere [25].

As an illustration, we have plotted in Figs. 4(a) and 4(b) the most important modified radial couplings [see Eq. (17)] and in Figs. 4(c) and 4(d) some rotational ones [Eq. (18)]. The main mechanism of reaction (1) at low energy involves transitions between $1\,^3\Pi$ and $8\,^3\Pi$ in the neighborhood of $R \simeq 6.5a_0$ and $3.25a_0$ [see the avoided crossings in Fig. 1 and the two peaks in the corresponding coupling in Fig. 4(a)], and $1-9\,^3\Sigma^+$ and $1-9\,^3\Pi$ avoided crossings at $R \simeq 2.25a_0$ in Fig. 1 [see the single peaks of the corresponding couplings in Fig. 4(a)]. These transitions are strongly affected by $1\,^3\Sigma^+-8\,^3\Pi$ rotational couplings, Fig. 4(c). For reaction (2), the mechanism at low energy involves transitions between states $2\,^3\Sigma^--13\,^3\Sigma^-$ at $R \simeq 8.1a_0$ and $2\,^3\Pi-11\,^3\Pi$ at $R \simeq 6.1a_0$ [see the radial couplings in Fig. 4(b) and rotational ones in Fig. 4(d)].

IV. DYNAMICAL RESULTS

A. Total EC cross section in $N^{2+}(2s^22p\,^2P^o)+H(1s)$ collisions

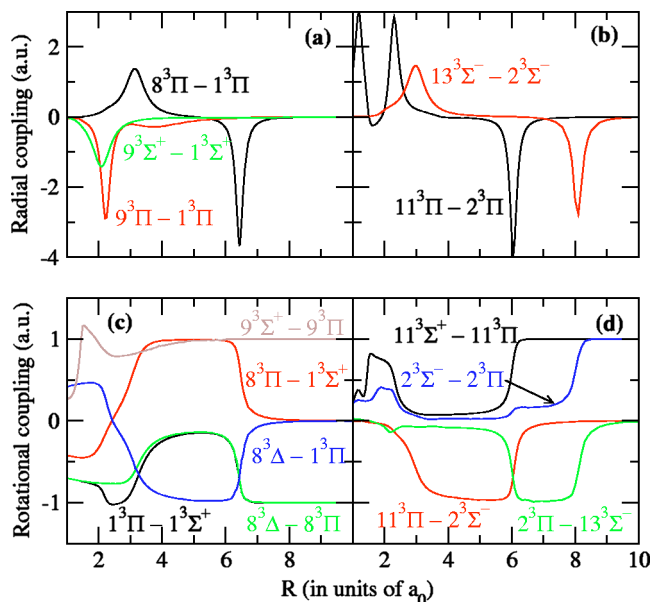We have calculated the total cross sections for the EC reaction (1) by employing a 56-term molecular basis set; this

basis includes the triplet and singlet states whose energies are plotted in Figs. 1 and 2, respectively. The above mentioned cross section is obtained as

$$\sigma = \frac{1}{12}[\sigma(1\,^1\Sigma^+) + \sigma(1\,^1\Pi_+) + \sigma(1^1\Pi_-)] + \frac{3}{12}[\sigma(1\,^3\Sigma^+) + \sigma(1\,^3\Pi_+) + \sigma(1^3\Pi_-)], \quad (22)$$

where $\sigma(i)$ are the cross sections obtained for the capture reaction with initial channel i. Our cross sections (tabulated values are available at [27]) are compared in Fig. 5 with experimental results and previous theoretical values. We have restricted the energy range to $E<300$ keV, where ion-
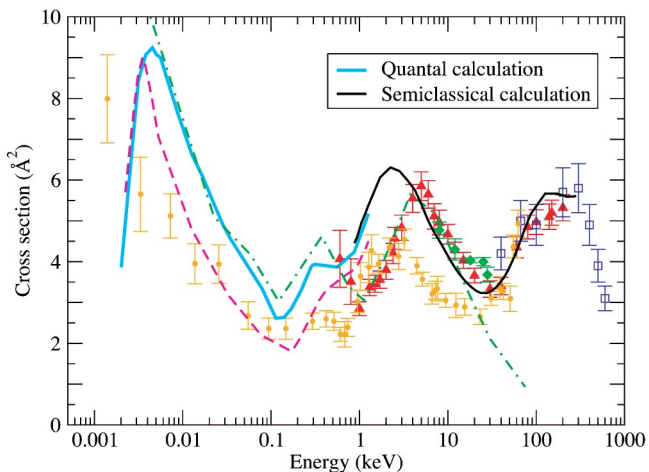

FIG. 5. Total EC cross sections in $N^{2+}(2s^22p\,^2P^o)+H(1s)$ collisions [reaction (1)]. Present calculations, — semiclassical calculation; — quantal calculation. Experimental results, □ [3]; ◆ [4]; ▲ [5]; ● [6]. Theoretical results, –·–·– [8]; – – – [9].
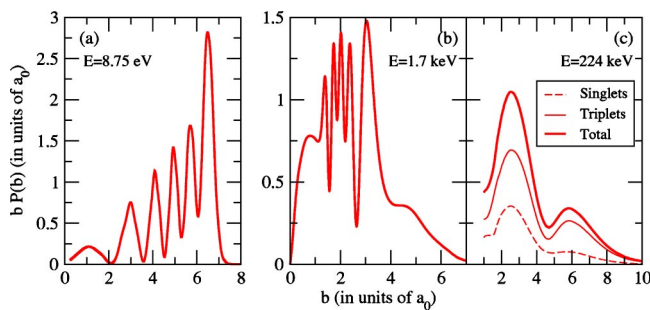
FIG. 6. $bP(b)$ as a function of b for EC in reaction (1) at three energies (labeled in the panels) showing three different mechanisms.
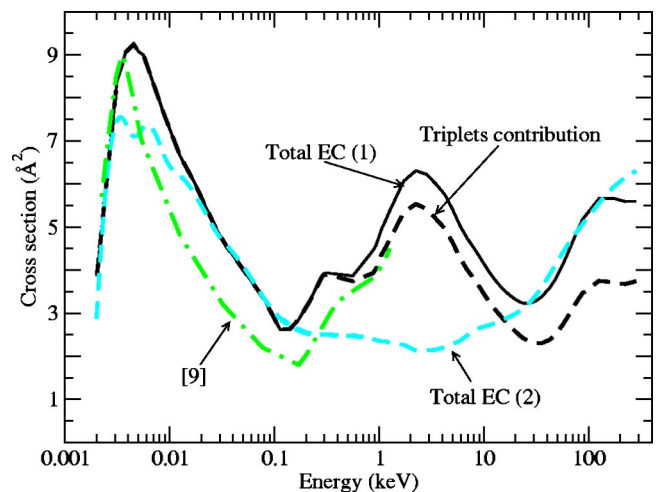

FIG. 7. Total cross sections for reactions (1) and (2), as indicated in the figure. The contributions of the triplet states to the total cross sections for reaction (1) and the results of Ref. [9] are also included. For $E < 1$ keV, the cross sections have been calculated using the quantal treatment and the semiclassical one for $E > 1$ keV.

ization starts to compete with EC [26]. The calculated total cross sections of Fig. 5 show three maxima, which are located at $E \simeq 4$ eV, 2 keV, and 200 keV, respectively; these maxima correspond to three mechanisms which are discussed below.

The low-energy mechanism, as already explained by Herrero *et al.* [9], is the transition in the avoided crossings between the molecular states dissociating into channels 1 and 8 at $R \simeq 6.4a_0$ (Fig. 1, bottom left panel); this mechanism is illustrated in Fig. 6(a), which shows the Stueckelberg oscillations, typical of the Landau-Zener model. To check the contribution of transitions in the 1-9 avoided crossing, we have carried out a 6-state $\{1\ ^3\Sigma^+, 1\ ^3\Pi_\pm, 9\ ^3\Sigma^+, 9\ ^3\Pi_\pm\}$ calculation with the dynamical couplings evaluated at closely spaced points in the avoided crossing region; this test yields values smaller than 0.11 Å^2 at the lowest energies considered in our calculation and, accordingly, it has been traversed diabatically. In practice, we have fitted the sharp peaks of the 1-9 radial couplings to Lorentzian functions, which have been subtracted from the calculated radial couplings, while the corresponding interaction matrix elements have been retained in the quantal calculation. This procedure also allows us to check the influence of the accuracy of our molecular data in the cross section by shifting the energy of the entrance channel to match the experimental asymptotic 1-9 energy difference. The two-state calculations with these shifted energies ($1\ ^3\Sigma^+ - 9\ ^3\Sigma^+$ and $1\ ^3\Pi - 9\ ^3\Pi$) yield cross sections smaller than 0.30 Å^2, remaining negligible compared to those produced by the 1-8 transitions.

In Fig. 5, we see that our results are systematically higher than those of the calculation of Herrero *et al.* [9]. To understand the reason for this, we have plotted in Fig. 7 the contribution of the triplet states to the total EC cross section, which shows that the contribution of the singlet states is negligible at $E < 400$ eV, and that the cross section of Ref. [9] agrees with our triplet contribution at $E > 600$ eV. Therefore, the difference between the two calculations is not a consequence of the approximation of Ref. [9] of neglecting the contribution of singlet states and must be due to small differences in the molecular wave functions, which become relevant at low impact energies. For instance, fitting the energies of states $1\ ^3\Pi$ and $8\ ^3\Pi$ near their pseudocrossing, we obtain the following Landau-Zener parameters (see [18] and references therein): $R_0 = 6.439a_0$ (crossing point), $a = 0.0256$ hartrees/a_0 (difference of slopes), and $H_{12} = 0.00182$ hartrees

(interaction), while those of Ref. [9] are $R_0 = 6.546a_0$, $a = 0.026$ hartrees/a_0, and $H_{12} = 0.00145$ hartrees. We have checked that the small difference in the value of H_{12} leads to an approximate factor of 1.3 in the cross section, in agreement with the results of the full calculation shown in Fig. 5. Since our energies are slightly lower than those of Ref. [9], and show better agreement with the spectroscopic atomic levels, we conclude that our calculation is more precise at low impact energies. As in Ref. [9], we obtain a maximum of the total cross section at $E \simeq 4$ eV, which is not found in the merged-beam experiments [6].

At $E \simeq 2$ keV, our total cross section shows a local maximum, while the maximum of the experimental data of Wilkie *et al.* [5] is shifted to $E \simeq 5$ keV, and agrees with the two-state calculation of Bienstock *et al.* [8]. On the other hand, for $E < 20$ keV, our cross section lies parallel to and is about 25% higher than that of Pieksma *et al.* [6]. In this energy range, the avoided crossings of the entrance channel at $R \simeq 6.4a_0$ are traversed diabatically, and the most important transitions take place near the avoided crossings at $R \simeq 3.25a_0$ and $R \simeq 2.25a_0$ to channels 8 and 9, respectively [see the peaks in the radial couplings of Fig. 4(a)]; this is illustrated in Fig. 6(b) for $E = 1.7$ keV.

To check our calculation in this energy region, we have studied the convergence of the molecular expansion. In Fig. 8(a) we compare the EC transition probabilities calculated with a (minimal) two-state basis $\{1\ ^3\Pi_+, 8\ ^3\Pi_+\}$, similar to that used in [8], an eight-state basis $\{1\ ^3\Sigma^+, 1\ ^3\Pi_\pm, 8\ ^3\Sigma^-, 8\ ^3\Pi_\pm, 8\ ^3\Delta_\pm\}$ that includes all the states of channels 1 and 8, with their radial and rotational couplings, and the whole basis (35 states) of the triplet subsystem. We can observe in this figure that, for $3.5 < b < 5a_0$, there is an important difference between the transition probabilities, and hence in the corresponding cross section, of the two-state and the eight-state calculations, which is mainly due to the influence of the rotational couplings of Fig. 4(c). A small change is found, however, on increasing the basis to 35 states. These results point
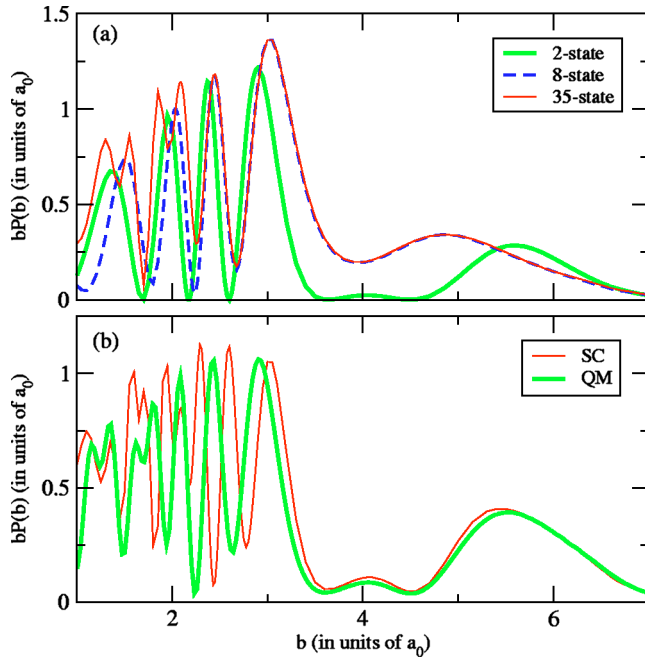
FIG. 8. $bP(b)$ for EC in $N^{2+}(2s^22p\ ^2P^o)+H(1s)$ collisions. (a) Contribution of the triplet subsystem for $E=1.26$ keV, calculated with 2-,8-, and 35-state molecular basis sets, as indicated in the figure. (b) $bP(b)$ for EC at $E=560$ eV. Lines are labeled in the figure: SC stands for the semiclassical calculation and QM stands for the quantal one.

out that the calculations for the total EC cross section and, in particular, for the cross section for formation of $N^+(2s2p^3\ ^3D^o)$ (channel 8) are correctly described with our basis, while the two-state calculation is not converged. Therefore, the good agreement between the experiment of Wilkie *et al.* [5] and the two-state model of Bienstock *et al.* [8] should be taken as fortuitous.

With respect to the validity of the semiclassical treatment at this intermediate energy region, we have found that quantal and semiclassical cross sections, as shown in Fig. 5, and transition probabilities, are practically identical for $E>1$ keV. At lower energies, there are sizable differences between the two calculations; this is illustrated in Fig. 8(b), where we plot the values of $bP(b)$ vs b for the EC process with entrance channel $1^3\Pi_-$ at $E=560$ eV. We see in Fig. 8(b) a shift of the maxima of the transition probabilities, which was also found in a similar comparison for EC in $Be^{4+}+H$ collisions [16].

Finally, for energies between 5 and 300 keV, Fig. 5 shows that our results are in very good agreement with the measurements of Refs. [3–5]. At high energies ($E>20$ keV), triplet states dissociating into channels 5 and 11 and singlet states dissociating into channels 6, 7, 10, and 12 become accessible. This leads to the two-peak structure of the transition probabilities shown in Fig. 6(c): the outer peak, in both the singlet and triplet subsystems, is produced by transitions to higher (in energy) channels (11, 10, and 12) while transitions to lower (in energy) channels (5, 6, and 7) produce the inner peak.
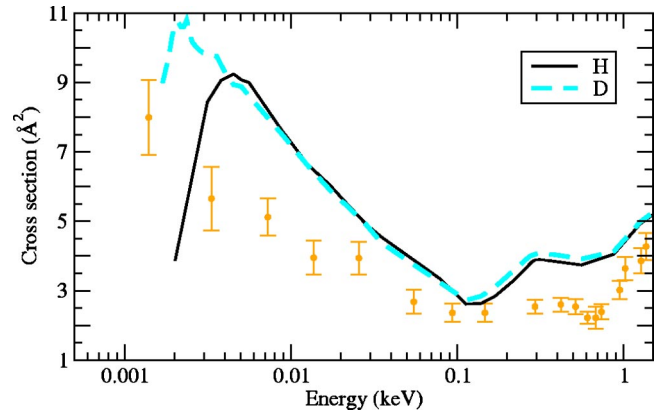

FIG. 9. Comparison of EC total cross sections in collisions $N^{2+}(2s^22p\ ^2P^o)$ with $H(1s)$ and $D(1s)$, as indicated in the figure. ●, experimental results of [6] for N^{2+} collisions with D.

B. Isotopic dependence

Since merged-beam experiments are carried out using a D target, while the results shown in Fig. 5 considered collisions with H, it is useful to study the isotopic dependence of the cross sections. To illustrate this effect, we compare in Fig. 9 the EC total cross section from H and D, which shows a significant isotopic effect only for $E<10$ eV, but the maximum at low impact energies is obtained for both targets. One can also note in this figure a small, but nevertheless surprising, isotopic dependence in the region $100<E<500$ eV. To explain this unexpected effect, we have compared in Fig. 10 the transition probabilities for EC in collisions with both isotopic species at $E=35$ and 140 eV. As we have already mentioned, at $E<100$ eV, the dominant mechanism involves transitions in the pseudocrossing region at $R\simeq6.4a_0$. At $E>100$ eV, transitions at $R\simeq3.0a_0$ start to be noticeable, leading to the peaks at $b<3.0a_0$ (see Fig. 10, $E=140$ eV). Since trajectory effects, which depend on the nuclear masses, are more important for trajectories with small b, this explains the apparent paradox of more important isotopic dependence at relatively higher energies.

C. Total EC cross section in $N^{2+}(2s2p^2\ ^4P)+H(1s)$ collisions

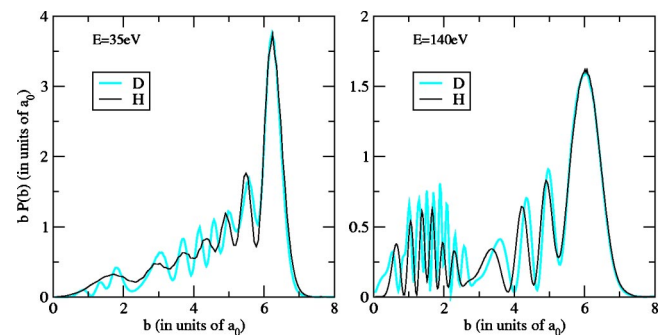Total cross sections for reaction (2) are obtained with the relation

FIG. 10. $bP(b)$ as a function of b [see Eq. (21)] for electron capture in collisions $N^{2+}(2s^22p\ ^2P^o)+H(1s)$ and $N^{2+}(2s^22p\ ^2P^o)+D(1s)$, at the impact energies indicated in the figure.
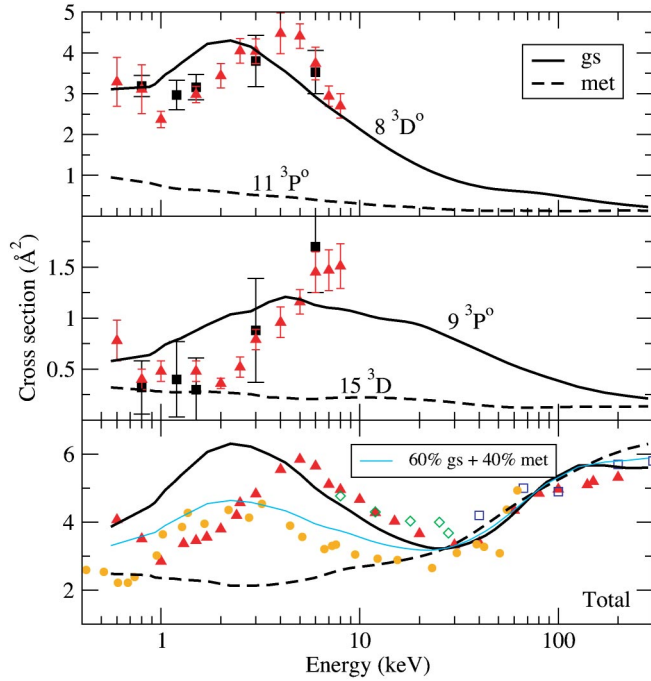
FIG. 11. Partial EC cross sections in $N^{2+}+H(1s)$ collisions from $N^{2+}(2s^22p\,^2P^o)$ (gs) and $N^{2+}(2s2p^2\,^4P)$ (met) initial states for populating $N^+(2s2p^3\,^3D^o)$ and $N^+(2s2p^3\,^3P^o)$, as indicated in the figure. In the bottom panel, we plot the total EC cross sections in the same energy range. In this panel the theoretical results are — cross section for reaction (1); – – – cross section for reaction (2); — cross section obtained for a beam containing 40% of metastable $N^+(2s2p^2\,^4P)$ and 60% of ground state $N^{2+}(2s^22p\,^2P^o)$ ions. Experimental results □ [3]; ◇ [4]; ▲ [5]; ■ [2]; ● [6].

$$\sigma = \frac{1}{8}\left[\sigma(2\,^3\Sigma^-) + \sigma(2\,^3\Pi_+) + \sigma(2\,^3\Pi_-)\right] + \frac{5}{24}\left[\sigma(2\,^5\Sigma^-)\right.$$

$$\left. + \sigma(2\,^5\Pi_+) + \sigma(2\,^5\Pi_-)\right], \tag{23}$$

where the notation is similar to that of Eq. (22). We have employed in this calculation the set of 35 triplet states also used for reaction (1), and 15 quintet molecular states. The ensuing cross sections are plotted in Fig. 7. At $E<0.1$ keV and $E>30$ keV, the cross sections for reactions (1) and (2) show similar values and energy dependences, indicating that a contamination of the initial beam by metastable ions would be unnoticeable by comparing experimental and theoretical total EC cross sections. On the contrary, for $0.1<E<30$ keV, the presence of metastable ions in the experiment would be more easily noticed in the total cross section. In this respect, the good agreement of our total cross section for reaction (1) with the experiments of Refs. [3–5] for $E>5$ keV indicates that there was a very small proportion of metastable N^{2+} ions in the corresponding initial beams. On the other hand, the disagreement of the cross section measured in [6] with other data in the region $0.1<E<30$ keV might be attributed to a larger proportion of metastable ions in that experiment. However, as shown in the bottom panel of Fig. 11, a proportion of 40% of metastable ions is required to get good agreement with the experi-
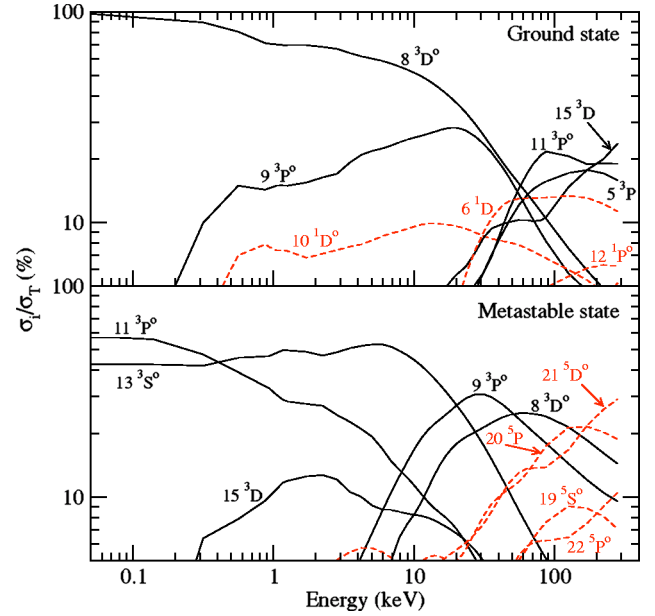

FIG. 12. Branching ratio to electron capture channels in reactions (1) and (2). N^+ products are indicated in the panels.

ment of Pieksma *et al.* [6], who did not find any evidence of such a high proportion of metastable ions. Nevertheless, we can observe good agreement between all experiments and our calculation for $E>30$ keV, where the cross sections for reactions (1) and (2) are very similar. On the other hand, the shift of the maximum ($E \simeq 2$ keV) of the cross section in our calculation with respect to that of the experiment of Wilkie *et al.* ($E \simeq 5$ keV) (see Fig. 11) cannot be related to the possible presence of metastable ions.

D. State-selective EC cross sections

We compare in Fig. 11 the partial cross sections for population of states $8\,^3D$ and $9\,^3P^o$ through reaction (1) with the experimental values of [5,2]. We also include the partial cross sections for populating $11\,^3P^o$ and $15\,^3D$ channels with reaction (2) because they would produce peaks overlapping with the previous ones in the energy change spectrum.

Although we find a reasonable agreement, a shift, similar to that found for the total cross section (see also the bottom panel of Fig. 11), can be noticed in this figure, which is not surprising given that the experimental total cross section was used to obtain the partial ones in those works. Cross sections for several exit channels and in an extended energy range are presented in Fig. 12, where we plot the contribution ratio of the individual channels, calculated as

$$\gamma_i = \frac{\sigma_i}{\sum_j \sigma_j} \times 100, \tag{24}$$

with i and j running over the EC channel index.

The relative values of the partial cross sections of Fig. 12 for reaction (1) can be qualitatively explained by taking into account only transitions from the entrance channels. As we have already discussed, reaction (1) takes place through tran-

sitions to states of channel 8. At high v, other triplet states (channels 5 and 11) are populated. In the case of reaction (2) and at low v, the dominant exit channels ($11\,^3P^o$ and $13\,^3S^o$) are populated in the avoided crossings at $R \simeq 6.1a_0$ and $8.1a_0$, respectively. The ratios of Fig. 12 are due to the initial statistical mixture: the states correlating with $11\,^3P^o$ are populated in the avoided crossing at $R \simeq 6.1a_0$, which appears in the $^3\Pi$ subsystem, whose statistical weight is 2/8, while the state correlating with $13\,^3S^o$ is populated in the avoided crossing at $R \simeq 8.1a_0$ in the $^3\Sigma^-$ subsystem, with a statistical weight of 1/8. At $E > 1$ keV, the avoided crossings at large R are traversed diabatically, and the main transitions take place at $R \simeq 3a_0$ via the maximum of the $2\,^3\Sigma^- - 13\,^3\Sigma^-$ coupling (see Fig. 4), which leads to a dominant population of the channel $13\,^3S^o$. As in the case of reaction (1), for energies above 10 keV, other channels ($9\,^3P^o$, $8\,^3D^o$, $20\,^5P$, $21\,^5D^o$ become accessible).

V. CONCLUSIONS

We have calculated state-selected EC cross sections in collisions of N^{2+} in ground ($2s^22p\,^2P^o$) and metastable ($2s2p^2\,^4P$) states with $H(1s)$ and $D(1s)$, by employing a molecular expansion with *ab initio* molecular wavefunctions, and quantal and semiclassical treatments. The use of the quantal approach has allowed us to gauge the isotopic dependence of the cross section and the accuracy of the semiclassical eikonal approach. Our calculations yield very similar cross sections for reactions (1) and (2) with the exception of the energy region 0.2–30 keV, where the comparison of our results with the values of Refs. [4,5] does not show a noticeable contamination by metastable ions in those experiments.

At low $E(E < 1$ keV$)$, we have reproduced the energy dependence and the maximum at $E \simeq 4$ eV of the calculation of [9] for reaction (1). One result of our calculation is the branching ratios for populating different EC channels. We have found that the EC from $N^{2+}(2s^22p\,^2P^o)$, and at energies lower than 40 keV, involves the simultaneous excitation of one projectile electron, leading to $N^+(2s2p^3\,^3D^o)+H^+$. Several collision channels are formed at higher energies. In the collision of metastable $N^{2+}(2s2p^2\,^2P)$, the dominant EC channels are, at low energies, $N^+(2s^22p3s\,^3P^o)+H^+$ and $N^+(2s2p^3\,^3S^o)+H^+$.

[1] D. Voulot, D. R. Gillen, W. R. Thompson, H. B. Gilbody, R. W. McCullough, L. Errea, A. Macías, L. Méndez, and A. Riera, J. Phys. B **33**, L187 (2000).

[2] D. Voulot, D. R. Gillen, D. M. Kearns, R. W. McCullough, and H. Gilbody, J. Phys. B **34**, 1039 (2001).

[3] R. A. Phaneuf, F. W. Meyer, and R. H. McKnight, Phys. Rev. A **17**, 534 (1978).

[4] W. Seim, A. Müller, I. Wirkner-Bott, and E. Salzborn, J. Phys. B **14**, 3475 (1981).

[5] F. G. Wilkie, F. B. Yousif, R. W. McCullough, J. Geddes, and H. B. Gilbody, J. Phys. B **18**, 479 (1985).

[6] M. Pieksma, M. E. Bannister, W. Wu, and C. C. Havener, Phys. Rev. A **55**, 3526 (1997).

[7] T. G. Heil, S. E. Butler, and A. Dalgarno, Phys. Rev. A **23**, 1100 (1981).

[8] S. Bienstock, A. Dalgarno, and T. G. Heil, Phys. Rev. A **33**, 2078 (1986).

[9] B. Herrero, I. L. Cooper, A. S. Dickinson, and D. R. Flower, J. Phys. B **28**, 711 (1995).

[10] L. F. Errea, A. Macías, L. Méndez, I. Rabadán, and A. Riera, J. Phys. B **33**, L615 (2000).

[11] C. N. Cabello, L. F. Errea, L. Fernández, L. Méndez, A. Macías, I. Rabadán, and A. Riera, J. Phys. B **36**, 307 (2003).

[12] T. Mroczkowski, D. W. Savin, R. Rejoub, P. S. Krstić, and C. C. Havener, Phys. Rev. A **68**, 032721 (2003).

[13] T. G. Lee, A.-T. Le, and C. D. Lin, J. Phys. B **36**, 4081 (2003).

[14] M. H. Mittleman, Phys. Rev. **188**, 231 (1969).

[15] W. R. Thorson and J. B. Delos, Phys. Rev. A **18**, 117 (1978).

[16] L. F. Errea, C. Harel, H. Jouin, L. Méndez, B. Pons, and A. Riera, J. Phys. B **31**, 3527 (1998).

[17] L. F. Errea, L. Méndez, and A. Riera, J. Phys. B **15**, 101 (1982).

[18] B. H. Bransden and M. H. C. McDowell, *Charge Exchange and the Theory of Ion-Atom Collisions* (Clarendon, Oxford, 1992).

[19] L. F. Errea, C. Harel, H. Jouin, L. Méndez, B. Pons, and A. Riera, J. Phys. B **27**, 3603 (1994).

[20] A. Riera, Mol. Phys. **88**, 199 (1996).

[21] E. Davidson, in *MOTECC, Modern Techniques in Computational Chemistry*, edited by E. Clementi (ESCOM Publishers, Leiden, 1990).

[22] C. E. Moore, *Atomic Energy Levels*, Nat. Bur. Stand. Ref. Data Ser., Nat. Bur. Stand. (U.S.) Circ. No. 35 (U.S. GPO, Washington, DC, 1971), Vol. 1.

[23] P. O. Widmark, P. Malmqvist, and B. Roos, Theor. Chim. Acta **77**, 291 (1990).

[24] J. F. Castillo, L. F. Errea, A. Macías, L. Méndez, and A. Riera, J. Chem. Phys. **103**, 2113 (1995).

[25] L. F. Errea, L. Fernández, L. Méndez, A. Macías, I. Rabadán, and A. Riera, J. Chem. Phys. **121**, 1663 (2004).

[26] M. B. Shah and H. B. Gilbody, J. Phys. B **14**, 2831 (1981).

[27] http://tcam.qui.uam.es/publicaciones.